Materials Advances

ROYAL SOCIETY OF CHEMISTRY

PAPER

View Article Online
View Journal | View Issue

Cite this: *Mater. Adv.*, 2026, 7, 1508

An edible microbial cellulose-based triboelectric nanogenerator: a sustainable approach for energy harvesting

Raj Ankit,[a] Simranjeet Kaur,[b] Shinar Athwal,[c] Taranveer Kaur[d] and Jayant Kolte *[a]

The demand for sustainable energy has been increasing, driving the exploration of novel materials for sustainable energy-harvesting technologies. The present study explores a triboelectric nanogenerator (TENG) based on microbial cellulose (MC), synthesized by symbiotically cultured bacteria and yeast (SCOBY), as a positive triboelectric material, and fluorinated ethylene propylene (FEP) as a negative triboelectric material. The MC film synthesized by a simple fermentation method exhibits very high porosity and a highly rough surface, making it an excellent triboelectric material. The fabricated TENG exhibits an open-circuit voltage (V_{oc}) of ~620 V, a short-circuit current (I_{sc}) of ~40 μA, and a power density of 16.5 W m^{-2} at a 10 MΩ load resistance, demonstrating its superior performance compared to reported bacterial-cellulose-based TENGs. Moreover, the synthesized MC film exhibits efficient antibacterial activity against Gram-negative and Gram-positive bacteria, without the need for an additional antibacterial agent. This study fills a gap in research into clean and green energy harvesting using MC, creating an opportunity for novel, environmentally-friendly TENGs. Practical applications, such as powering a calculator, validate the potential for commercial use of innovative TENG technologies.

Received 14th October 2025,
Accepted 5th December 2025

DOI: 10.1039/d5ma01186h

rsc.li/materials-advances

1. Introduction

Energy is the foundation for technological advancements, modern civilization, and the socio-economic growth of the current era. The exploitation of traditional energy resources has led to environmental pollution and global climate change. This exhausts current fossil fuel resources, and there is an urgent need to explore sustainable and renewable energy sources.[1] Among the various sustainable methods of energy harvesting, Triboelectric nanogenerators (TENGs) have emerged as a promising, innovative solution due to their high efficiency, versatility, and cost-effectiveness. TENGs are based on the triboelectric effect, in which certain materials become electrically charged after coming into contact with each other and then separating.[2,3] This phenomenon can be used to generate electricity from mechanical movements, such as walking, running, and vibrations, as well as from environmental motions, such as wind and waves.[4–6] The TENG operates in four modes: vertical contact-separation mode, lateral sliding mode, single-electrode mode, and free-standing triboelectric-layer mode,[7–9] demonstrating its adaptability across various conditions and applications.

In recent years, there has been growing interest in the use of sustainable, biocompatible materials for the fabrication of TENGs to align with eco-friendly paradigms.[10,11] The integration of natural polymers into TENGs not only improves environmental sustainability but also enhances functionality and biocompatibility. Biopolymers such as natural rubber, poly(lactic) acid, chitosan, and cellulose are commonly used in the fabrication of biopolymer-based TENGs due to their biodegradability and renewable sources.[12–16] Several innovative techniques are also used to optimize the functional and structural designs of biopolymers in TENGs to improve efficiency and expand application scope.[13–15,17] Among naturally-derived materials, cellulose is the most abundant and renewable polymer, with great potential.[18] Cellulose is a complex polysaccharide with a chain-like structure[19] and the chemical formula $C_6H_{10}O_5$.[20] Cellulose exhibits excellent dielectric properties and shows superior electrical response to mechanical energy.[21] Furthermore, Cellulose contains multiple oxygen atoms, which endow it with electron-donating properties—making it an excellent candidate for the positive friction material in polymer-based TENGs.[22,23] Various advancements, such as structural innovations and chemical functionalization, have been implemented in cellulose-based TENGs. A multi-fluid electrospinning technique has been used to fabricate a composite of cellulose nanocrystals/cyanoethyl

[a] Department of Physics and Materials Science, Thapar Institute of Engineering and Technology, Patiala, Punjab, 147004, India. E-mail: jayantkolte@thapar.edu; Fax: +91-175-2393020; Tel: +91-175-2393116
[b] Department of Physics, Punjabi University, Patiala, Punjab, India
[c] Department of Biotechnology, Thapar Institute of Engineering and Technology, Patiala, Punjab, India
[d] Department of Science, Public College Samana, Patiala, Punjab, India

cellulose (CEC)/polyvinylidene fluoride (PVDF), which enhances triboelectric output performance, achieving an open-circuit voltage of 10.01 V and a short-circuit current of 3.30 μA.[24] Composites of polydopamine and cellulose nanofibrils (PDA/CNF) demonstrate their potential as self-powered sensors, increasing output performance by 20 times to 205 V and 20 μA.[25] Cellulose paper-based TENGs use multi-layer forming technology to achieve an open-circuit voltage of 227.1 V and operate even under harsh conditions.[26]

Among various types of celluloses, microbial cellulose (MC) is the most beneficial due to its natural abundance, excellent flexibility, sustainability, and biodegradability. It is mostly produced by certain bacteria.[27] Microbial cellulose has a three-dimensional nanofibrillar morphology,[28] providing excellent mechanical strength, moderate density, and high purity.[29] It has a high water-absorption capacity, a large surface area, and moldability.[30] A symbiotic culture of bacteria and yeast (SCOBY) consists of various bacteria and yeast, such *as Acetobacter Aceti*, *Gluconobacter oxydans, Zygosaccharomyces*, and *Saccharomyces*, which help in producing cellulose biofilm.[31] The biofilm formed by bacteria consists of very fine microfibrils that bind to plant cellulose. These microfibrils have good film-forming capacity and excellent flexibility. Along with these structural advantages, the MC's antibacterial properties are also important for TENG applications. When microbes grow on the surface of wearable biomedical devices that remain in contact with human skin for an extended period, they can cause both infection and performance problems. To ensure user safety and the long-term smooth operation of the system, materials with natural or artificial antibacterial properties are crucial.

Various studies have been conducted to analyze the antibacterial properties of cellulose derived from microbial cultures. Although microbial cellulose lacks inherent antimicrobial properties, it can serve as an effective carrier for antimicrobial agents due to its adaptable surface chemistry, porosity, and large surface area, which can inhibit microorganism growth.[32] Malmir *et al.*[33] combined bacterial cellulose with carbon quantum dots-Titanium dioxide nanoparticles, which acted as antimicrobial agents, making the film antibacterial. Similarly, Sim *et al.*[34] integrated bacterial cellulose with silver nanoparticles to develop an antibacterial film. Moreover, the tight network of nanofibers and the low nutrient content of the microbial film create an unsupportive environment for microbial growth.[35] The incorporation of antimicrobial properties into microbial cellulose significantly broadens its applicability in infection management and medical devices, while also promoting the development of biodegradable and environmentally friendly alternatives to synthetic antimicrobial materials.

The present work introduces a self-sustaining, edible, and antibacterial MC-based triboelectric nanogenerator (MC-TENG). A triboelectric nanogenerator based on microbial cellulose as the positive triboelectric material, paired with fluorinated ethylene propylene (FEP) as the negative triboelectric material, has been developed. The conducting copper tape has been used as an electrode for the cellulose and FEP film, and the real-life applications are explored. The flexible, inherently oxygen-rich, and non-fibrillar structure of MC can significantly enhance triboelectric output and exhibit intrinsic antibacterial properties without the need for external additives. The membrane surface morphology is examined by Scanning Electron Microscopy (SEM), while Fourier Transform Infrared Spectroscopy (FTIR) is used to analyse its molecular structure. The antibacterial properties of the synthesized cellulose have been investigated, and it has been found to be self-reliant in its antibacterial activity. Moreover, the synthesized microbial cellulose exhibited inherent antibacterial properties, unlike most bacterial cellulose, thereby eliminating the need for antimicrobial agents and making the biomaterial self-reliant in its antibacterial activity. The present study aims to bridge the gap between antimicrobial development and sustainable energy harvesting, demonstrating dual-functional MC-based TENGs. The proposed TENG fills a crucial gap in sustainable energy-harvesting technologies by leveraging the inherent properties of microbial cellulose and demonstrates its practical feasibility.

2. Experimental

2.1. Materials

Apple cider vinegar, SCOBY bacteria, Conductive Copper tape (3M), and Fluorinated ethylene propylene (FEP)(TESSERACT) were purchased from Amazon. Sugar and green tea were procured from the local market.

2.2. Synthesis of microbial cellulose

Two tea bags were added to 1 L of boiling water and brewed for 15 minutes. After that, 200 g of sugar was added and stirred until dissolved, and the water was allowed to reach room temperature. Then, 200 mL of apple cider vinegar was added and stirred. Finally, the SCOBY culture was added, the container was covered with air-permeable cotton cloth, and it was left for 15 days. After 15 days, a thick layer forms on top of the solution. This cellulose layer was washed with cold soapy water and then dried at 50 °C in an oven. The flowchart for the synthesis of microbial cellulose is depicted in Fig. 1.

2.3. Fabrication of the microbial cellulose-based TENG

A 2 × 2 cm^2 piece of synthesized cellulose film was used as the positive triboelectric layer. A commercially available 2 × 2 cm^2 film was used as a negative triboelectric counterpart to form the microbial cellulose triboelectric nanogenerator (MC-TENG) based on triboelectric pairs of cellulose and FEP. Conducting copper tape was used as an electrode for both materials, as shown in the supplementary Fig. S1. A 1-cm separation was maintained between the MC and FEP layers during all measurements.

2.4. Antibacterial testing of microbial film

The antibacterial activities of the microbial film were investigated against *Escherichia coli* (*E. coli*), a Gram-negative model bacterium, and *Bacillus subtilis*, a Gram-positive model bacterium. For growth media, 2 g of Luria-Bertani (LB) and 2 g of agar

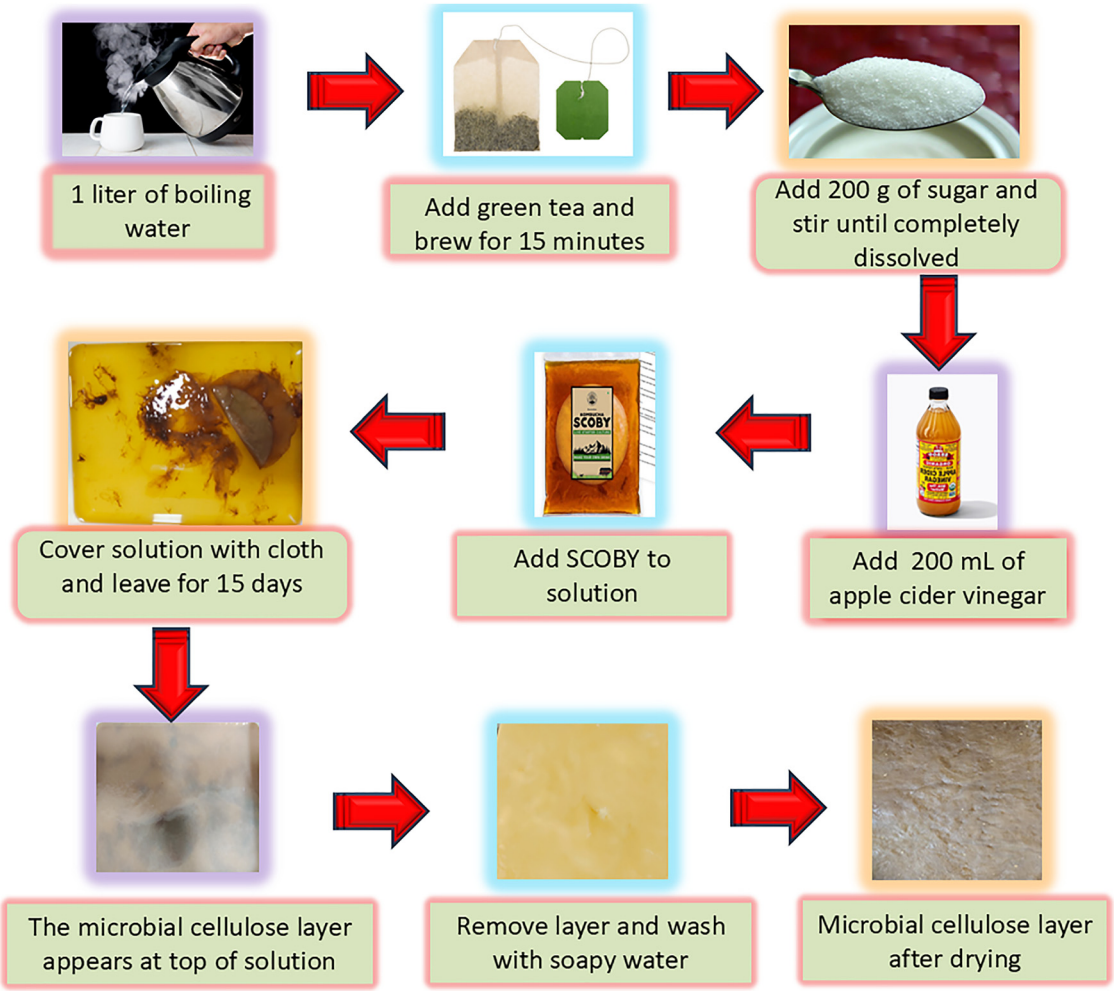

Fig. 1 Flow chart depicting the detailed synthesis of microbial cellulose.

were mixed in 100 mL of water and autoclaved at 121 °C for 15 minutes. After autoclaving, the growth media were poured into petri dishes and left to solidify for 15 minutes. Next, 100 μL of the bacterial culture was spread onto each agar plate. The UV-sterilized film was then placed on the agar plates. Finally, the plates were incubated at 37 °C for 24 hours, and the antibacterial activity of the film was determined by measuring the zone of inhibition.

2.5. Characterization

X-ray diffraction (XRD) data for the samples were collected on a SmartLab SE (Rigaku) instrument over a 20–90° scan range. A Field-effect scanning electron microscope (FE-SEM; Carl Zeiss Sigma 500) was used to study the morphology of the synthesized fibers. To understand the functional groups and chemical structure, Fourier-transform infrared (FTIR) spectroscopy (PerkinElmer Spectrum IT-FTIR; 500–4000 cm^{-1}) was used. Two different materials with an active area of 2 × 2 cm^2 were fixed at the two terminals of a standard linear motor-based testing system for the contact-separation process. The open-circuit voltage was measured by a digital oscilloscope (SIGLENT SDS1104X-E, impedance = 1 MΩ), and the short-circuit current of TENG was measured by an electrometer (Keithley 6517B). All the electric measurements were recorded at room temperature.

3. Results and discussion

3.1. XRD and dielectric analysis of MC film

In cellulose, the amorphousity arises from disordered chain segments, while the intra- and intermolecular hydrogen interactions of the cellulose chains contribute to a partly crystalline structure. The ratio between these amorphous and crystalline regions significantly affects the mechanical and functional properties of cellulose. Fig. 2(a) depicts the XRD analysis of the MC film recorded between 10 and 90° (2θ range). The crystallinity index (CrI) and the degree of crystallinity of the fabricated film were calculated using the Segal method[36] by using eqn (1) and (2). In the case of MC, two peaks are observed at 17° and 23°, corresponding to the (101) and (002) planes of cellulose, respectively.

$$\mathrm{CrI} = \frac{I_{002} - I_{\mathrm{am}}}{I_{002}} \times 100 \quad (1)$$

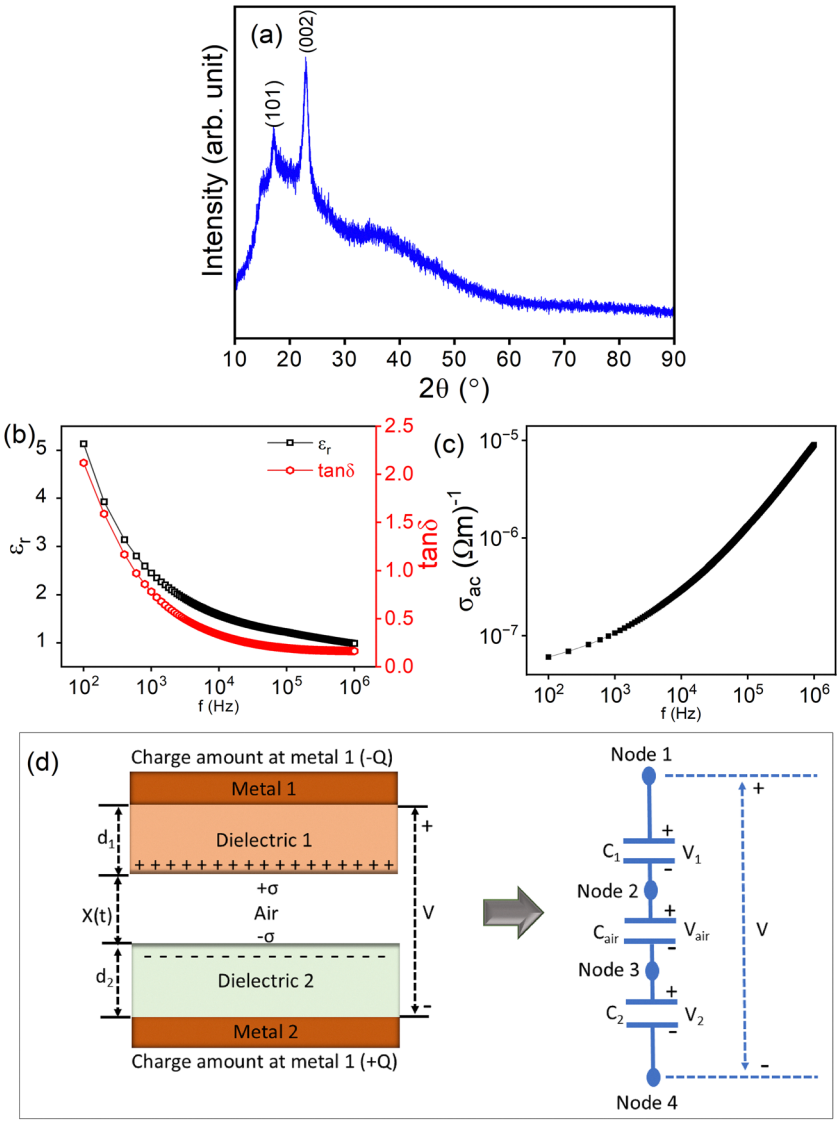

Fig. 2 (a) X-ray diffraction analysis, (b) dielectric constant and loss tangent, (c) AC conductivity *versus* frequency plots of MC film, (d) schematic diagram of dielectric-to-dielectric based TENG in contact separation mode with an equivalent circuit model of TENG.

$$\text{Degree of crystallinity} = \frac{I_{002}}{I_{002} - I_{\text{am}}} \quad (2)$$

where I_{002} is the maximum intensity of the diffraction peak, and I_{am} is the peak intensity around 20°, representing the amorphous part of cellulose. The CrI is found to be 40% and the degree of crystallinity is 2.5.[36]

The performance of the TENG has a direct relationship to the dielectric property of the triboelectric materials. The enhancement in the dielectric constant can substantially increase charge-trapping capability, reduce charge dissipation rate at the surface, and increase the surface charge density of the dielectric specimen—leading to enhanced output performance of the TENGs.[37]

Fig. 2(b) and (c) represent the frequency-dependent dielectric and conductivity response of the MC film measured from 100 Hz to 1 MHz at room temperature. The dielectric constant is obtained using the relation as:

$$\varepsilon_{\text{r}} = \frac{Cd}{\varepsilon_{\text{o}} A} \quad (3)$$

where C is capacitance of the sample, d is thickness, A is area, and ε_{o} is permittivity of free space (8.85×10^{-12} F m^{-1}). The conductivity of the materials has been obtained by using the relation:[38]

$$\sigma_{\text{ac}} = 2\pi f \varepsilon_0 \varepsilon_{\text{r}} \tan\delta \quad (4)$$

where f, ε_{r} and $\tan\delta$ represents the angular frequency, dielectric constant, and dielectric loss tangent, respectively. The MC film shows a dielectric constant of 2.5 and a dielectric loss of 0.8 at 1 kHz, indicating the dielectric material's power loss and making it desirable for several practical applications.

In order to understand the role of the dielectric constant in TENGs, a schematic of a dielectric-to-dielectric-based TENG

and its equivalent circuit model is depicted in Fig. 2(d). The potential difference exists across the surfaces of two dielectric layers, the two electrodes, and the dielectric-to-electrode interfaces, justifying the equivalent circuit model as three capacitors connected in series. The output performance of a TENG operating in the contact-separation mode[37] can be analyzed using eqn (5).

$$V = \frac{\sigma X(t)}{\varepsilon_0} - \frac{Q}{S\varepsilon_0}\left(\frac{d_1}{\varepsilon_1} + \frac{d_2}{\varepsilon_2} + X(t)\right) \quad (5)$$

where σ is the surface charge density, Q is the charge induced on the surface of the dielectric material, d_1 and d_2 are the thicknesses of each dielectric material; ε_1 and ε_2 represent the permittivity of the dielectric materials, $X(t)$ is the separation gap between the materials, S is the surface area of the electrode and ε_0 is the permittivity of vacuum. Eqn (5) clarifies that the induced charge (Q) and the surface charge density (S) are the key parameters in the output performance of TENG, and the enhancement in dielectric constant can significantly enhance the σ, increasing the triboelectric outputs.

3.2. Structural and morphological analysis of MC film

Fig. 3(a) shows the FTIR spectra of microbial cellulose film. The bands corresponding to the major functional groups of the cellulose can be observed in this graph. The band appearing at 1020 cm^{-1} is assigned to the stretching of the C–O–C bonds within a pyranose ring structure.[39] The in-plane bending vibrations of the –O–H group cause the band to appear at 1240 cm^{-1}.[40] The stretching vibrations of the –C–H bond appear at 1350 cm^{-1}.[41]

The absorption band at 1640 cm^{-1} is assigned to the stretching vibrations of the carbonyl group of the cellulose.[42] The band at 2910 cm^{-1} originates because of the –C–H stretching.[43] The absorption band near 3290 cm^{-1} is the signature band of the stretching of the hydroxyl (O–H) group.[43] In addition, a small band at ~890 cm^{-1} also appears, which can be attributed to the β-1,4 bond vibrations of glucose polymers.[44]

The MC film synthesized by fermenting the SCOBY culture with sweetened tea was analyzed using FESEM and is shown in Fig. 3(b) and (c). The analysis includes surface morphology and porosity after drying the MC film at 50 °C. The MC film exhibits a highly irregular, rough surface, attributed to random deposition during fermentation. The image shows that the film has significant uneven features and numerous variations across its surface. Very high porosity was also observed in the MC film, with pores varying in size and shape. Due to these characteristics, it can be utilized in specific applications where the porosity and surface roughness are advantageous. That is why it is further tested as a tribopositive material in TENG, leveraging its unique morphological characteristics to enhance energy-harvesting efficacy.

3.3. Analysis of antibacterial properties of the microbial film

The bacterial inhibition diameter is used to determine the bacteriostatic ability of the microbial film. The tested samples with *E. coli* and *Bacillus subtilis* bacterial strains are shown in Fig. 4(a) and (b). The film's bacterial sensitivity is revealed by the clear zone around it. The clear area is referred to as the zone of inhibition, and it represents the area on the agar plate where microbes cannot grow due to the diffusion of the antibacterial agent into the agar, creating an unfavourable environment for the reproduction or growth of the microorganisms.[45]

The larger the inhibition zone diameter, the greater the antibacterial effectiveness of the film. MC film with *E. coli* bacteria

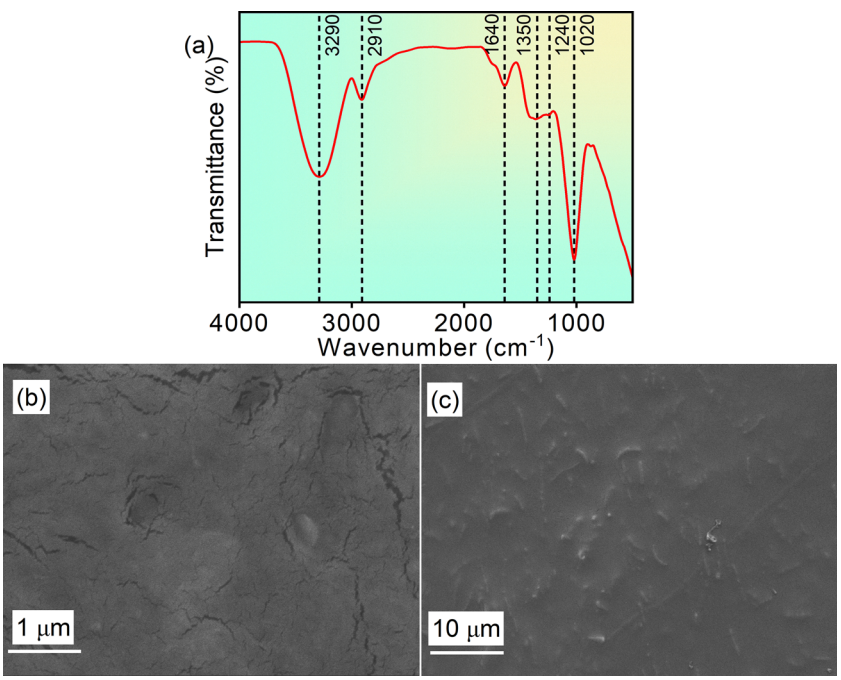

Fig. 3 (a) FTIR spectra and (b) & (c) Surface micrographs of the microbial cellulose film.

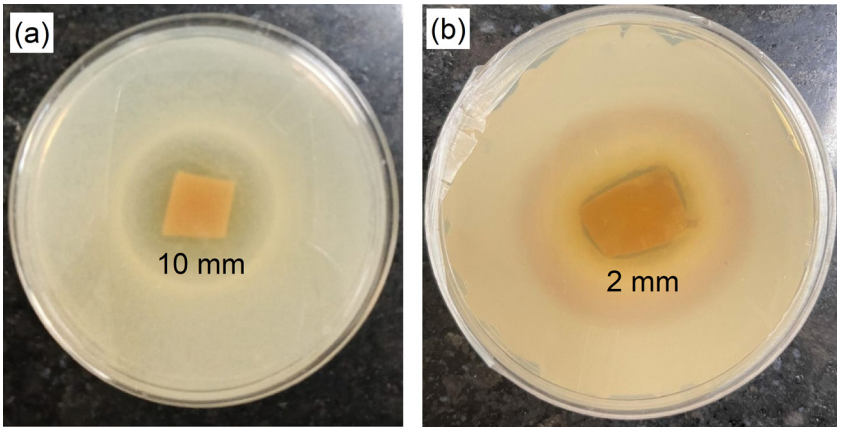

Fig. 4 Antibacterial activity of microbial film against (a) *E. coli* and (b) Bacillus.

shows a significant (~10 mm) inhibition zone, whereas for Bacillus it is only 2 mm. The results suggested that the film exhibited a strong antibacterial activity against Gram-negative bacteria and mildly inhibited the growth of Gram-positive bacteria. Moreover, even though the microbial film was not incorporated with other antimicrobial agents, it still exhibited antibacterial activity, which can be due to the source of the microbial film. The symbiotic culture of bacteria and yeast (SCOBY) comprises various bacteria and yeast, including *Acetobacter Aceti*, *Gluconobacter oxydans*, *Zygosaccharomyces*, and *Saccharomyces*.[31] The yeast species used, *i.e.*, Zygosaccharomyces and Saccharomyces, exhibit antibacterial activity by releasing proteins, peptides, and killer toxins (K1, K2, K28), which disrupt cellular processes and cell membrane integrity.[46] Thus, SCOBY-based cellulose film depicts a microbial cellulose film that inherently possesses antibacterial activity without the addition of other antibacterial agents. However, in the case of Bacillus, a uniform red-coloured ring formed around the film, which may be a compound released by the bacillus culture from the microbial film.

3.4. Working mechanism and overlapped electron cloud model of Microbial Cellulose-based MC-TENG device

The working mechanism of the microbial cellulose-based triboelectric nanogenerator (MC-TENG) is shown in Fig. 5(a) and (b). When an external force is applied to the nanogenerator, the upper and lower layers come into contact. The transfer of surface charge will occur due to contact electrification.

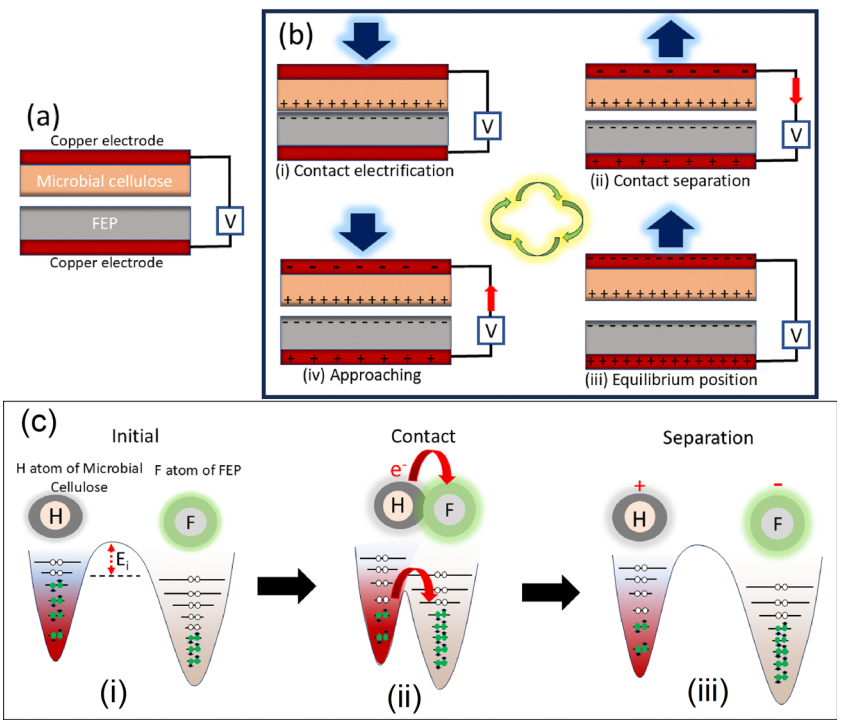

Fig. 5 (a) and (b) Working mechanism and (c)(i)–(iii) electron cloud model describing contact-electrification in MC-FEP for MC-TENG.

Cellulose is tribopositive, and FEP is tribonegative in the triboelectric series. It can be concluded that microbial cellulose is more likely to lose electrons while FEP gains electrons. Due to contact electrification, the positive charges gather on the surface of the cellulose film, while the negative charges are on the FEP polymer sheet (Fig. 5(b)(i)). As soon as both layers start separating due to external force, a potential difference is generated, as shown in Fig. 5(b)(ii). The potential difference keeps increasing with an increase in the separation gap until equilibrium (Fig. 5(b)(iii)) is attained. When the direction of the external force changes, the potential difference decreases with increasing separation distance between the two layers. Because of the electric potential difference, the electrons are compelled to move between the two layers, as the electrodes form a closed circuit. Due to electrostatic induction, the electrons will move in opposite directions from the source (Fig. 5(b)(iv)). Wang *et al.*[47] have explained these atomic interactions using an electron-cloud model. The possible physical process of electron transfer in contact electrification is shown in Fig. 5(c). Initially, as the MC and FEP are separated, the H atoms of MC and the F atoms of FEP are isolated, showing that no electron clouds are overlapping (Fig. 5(c)(i)). The atoms hold their electrons within the potential wells, and the interfacial potential barrier (E_i) prevents electron transfer between the electron clouds.

As soon as MC and FEP come into contact with each other, the H and F atoms of the interface enter into the repulsive area with the overlapping of clouds, reducing the interfacial potential barrier (Fig. 5(c)(ii)). At this stage, the contact electrification between the MC and FEP will occur because the electrons transfer easily into the potential well of the F atom at the interface of the polymer films. After this, when the layers get separated again, the H atom MC loses electrons, and the F atoms of FEP gain electrons. As a result of this, the contact surface of MC becomes positively charged while the contact surface of FEP becomes negatively charged (Fig. 5(c)(iii)). This continuous contact-and-separation mechanism on the MC generates a potential difference between the copper electrodes of both films, causing the external circuit to conduct current as charge flows.

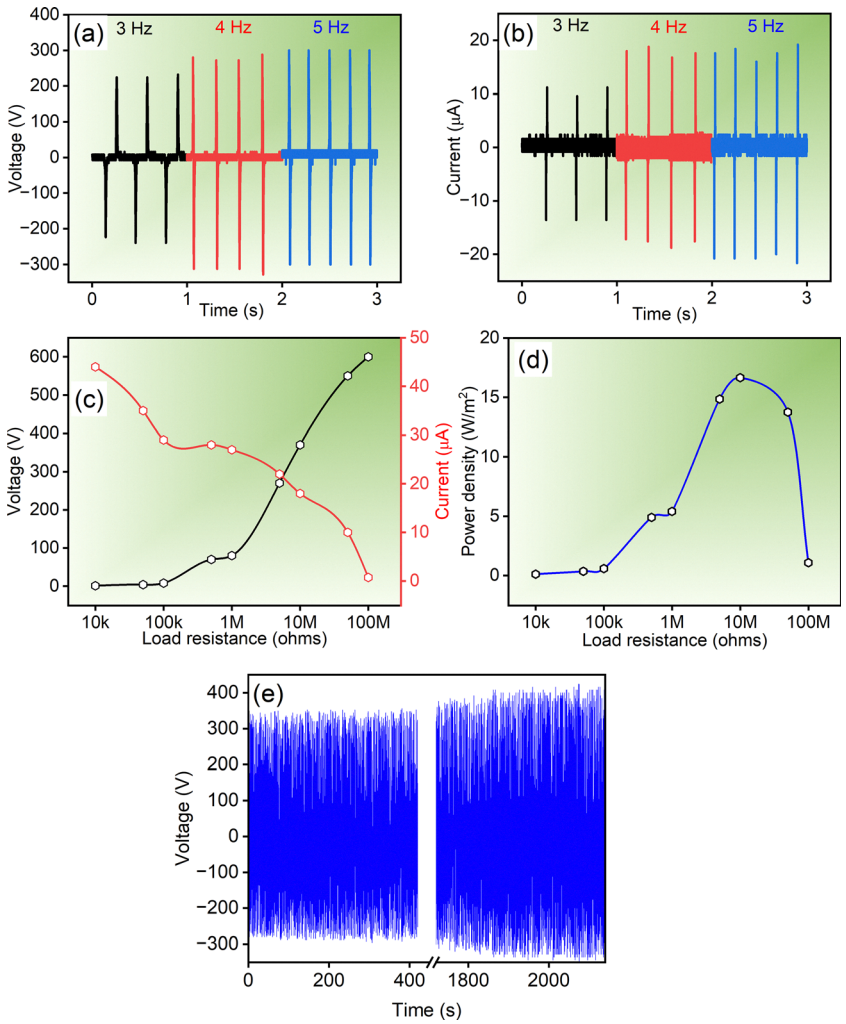

Fig. 6 (a) V_{oc} and (b) I_{sc} of fabricated TENGs using a linear-motor-based contact-separation mechanism. The measured (c) V_{oc} and I_{sc}, (d) power density on the external load resistance in the range of 10 KΩ to 100 MΩ of MC-TENG, (e) Stability measurement test of MC-TENG for more than 10 000 cycles.

Table 1 Literature summary of the bacterial cellulose-based TENGs

Tribopositive layer	Tribonegative layer	V_{oc} (V)	I_{sc} (μA)	Output power (W m^{-2})	Ref.
Bacterial cellulose (BC)/sodium alginate	FEP	300	27	1.81×10^{-3}	29
BC and barium titanate (BT)	PDMS	57.6	5.78	0.042	27
BC and BT	Copper tape	181	21	4.8	48
BC and carbon black grains	Ecoflex	102.3	2	—	49
MC	**FEP**	**620**	**40**	**16.5**	**Present work**

3.5. Testing of an effective output power density of CS/PVA-TENG

An MC film of size 2 × 2 cm^2 has been tested in MC-TENG for current (I) and Voltage (V) measurements. The electrical output of MC-TENG has been measured at three different frequencies: 3 Hz, 4 Hz, and 5 Hz by applying a compressive force of 1.5 N. Fig. 6(a) and (b) represents the measured open circuit voltage (V_{oc}) and short-circuit current (I_{sc}).

The MC-TENG exhibits a maximum voltage of ∼620 V (peak-to-peak) at approximately 4 Hz and a current of ∼40 μA (peak-to-peak) at approximately 5 Hz. Fig. 6(c) depicts the I_{sc} and V_{oc} values of MC-TENG measured at different load resistance values. As the load resistance increases, the current decreases,

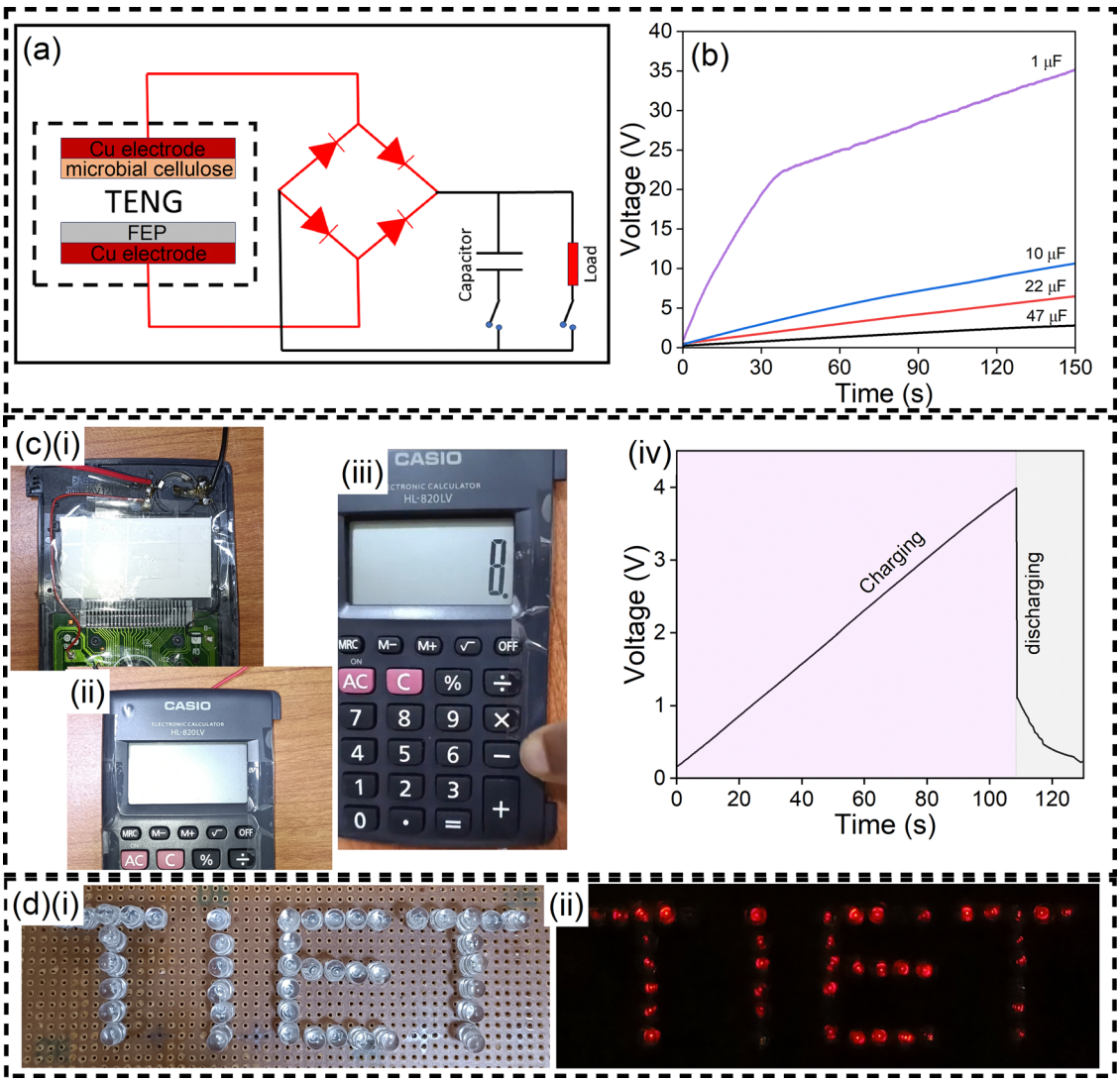

Fig. 7 (a) Equivalent circuit of the full-wave bridge rectifier for converting the alternating current signals of MC-TENG into the direct current signal to power up the electronic equipment by charging capacitors, (b) voltage accumulated across the capacitors having a capacitance of 1, 10, 22, and 47 μF. Photographic image of (c) (i) Calculator without any battery, (ii) calculator in switch off mode, (iii) calculator in switch on mode, (iv) charging and discharging of 22 μF capacitors for powering the calculator, (d) (i, ii) 55 red commercial LEDs connected in series spelt as 'TIET' was directly turned on by MC-TENG device.

while the voltage increases. The short-circuit and open-circuit conditions affect the output power density of any TENG. So, the power density is obtained by dividing the current and voltage values at different load resistances by the contact area, as depicted in Fig. 6(d). As expected, the MC-TENG exhibits lower power density at both lower and higher resistances. The MC-TENG achieved a maximum power density of 16.5 W m^{-2} at a load resistance of 10 MΩ. The increased output can be attributed to the film's high roughness and very high porosity. There are no reports available on such microbial cellulose-based TENG. The durability test was performed using a repetitive contact-separation test with more than 10 000 cycles, as shown in Fig. 6(e). On the other hand, very few reports are available on bacterial cellulose-based TENG. Table 1 represents triboelectric outputs of bacterial-cellulose-based TENGs reported to date.

3.6. Practical and real-time applications of the MC-TENG device

The electrical output o any TENG is an alternating signal, which is unsuitable for powering various portable and wearable electronic devices. Thus, a full-bridge rectifier has been connected to TENG to convert the alternating signal generated by TENG into a direct signal to charge capacitors. The electrical energy stored in the capacitor is then used to power the calculator.

The circuit diagram of the MC-TENG charging different capacitors is shown in Fig. 7(a). Different capacitors with capacitances of 1, 10, 22, and 47 μF were charged with the rectified voltage from the MC-TENG, and the accumulated voltages across the capacitors are shown in Fig. 7(b). As shown in Fig. 7(b), the 1-μF capacitor was charged to more than 35 V in 150 s. Finally, Fig. 7(c) shows the practical application of MC-TENG, using the electrical energy stored in the capacitor to power the calculator. Also, several red LEDs connected in series, spelt as ''TIET'', are turned on by contact separation of the MC-TENG without using any components such as rectifiers or capacitors, as shown in Fig. 7(d) and in supplementary video V1. As a result, these practical applications demonstrate the excellent efficiency of MC-TENG, which is synthesized and fabricated in a simple, cost-effective approach and can be easily used to power low-power, portable electronic equipment for commercial use.

4. Conclusion

This study effectively demonstrates the potential of MC as a tribopositive material in the fabrication of an environmentally friendly MC-TENG. Synthesized *via* a simple fermentation process, the fundamental characteristics of MC film, such as rough surface morphology and high porosity, improve the electrical outputs of TENG. The advantages of MC film, such as edibility, non-toxicity, and biodegradability, make it an exceptional material for sustainable energy applications. The MC-TENG exhibits an open-circuit voltage (V_{oc}) of ∼620 V, a short-circuit current (I_{sc}) of ∼40 μA, and a power density of 16.5 W m^{-2} at a 10 MΩ load resistance. Moreover, the biomaterial demonstrated remarkable inherent antibacterial activity against Gram-negative and Gram-positive bacteria with a zone of inhibition of 10 mm and 2 mm, respectively. In addition, the device's ability to charge the capacitor and power the calculator demonstrates its practical application.

Author contributions

Raj Ankit: conceptualization, visualization, synthesis, methodology, characterization, analysis, validation, writing – original draft, review, and editing. Simranjeet Kaur: synthesis, methodology, analysis, characterization writing – original draft. Shinar Athwal: conceptualization, methodology, analysis, validation, writing – original draft. Taranveer Kaur: characterization, analysis, validation, writing – original draft. Jayant Kolte: conceptualization, supervision, investigation, methodology, validation, writing – review and editing.

Conflicts of interest

The authors declare that they have no known competing financial interests or personal relationships that could have influenced the work reported in this paper.

Data availability

The data included in this article are available on request *via* the corresponding author. Supplementary information (SI) is available. See DOI: https://doi.org/10.1039/d5ma01186h.

Acknowledgements

The authors thank DST FIST (grant no. SR/FST/PS-II/2018/53) for providing characterization facilities.

References

1 S. Liang, *et al.*, The Recent Progress in Cellulose Paper-Based Triboelectric Nanogenerators, *Adv. Sustainable Syst.*, 2021, **5**(6), 2100034.
2 C. Wu, *et al.*, Triboelectric nanogenerator: a foundation of the energy for the new era, *Adv. Energy Mater.*, 2019, **9**(1), 1802906.
3 R. K. Rajaboina, U. K. Khanapuram and A. Kulandaivel, 2D Layered Materials Based Triboelectric Self-Powered Sensors, *Adv. Sens. Res.*, 2024, **3**(10), 2400045.
4 R. Dharmasena and S. Silva, Towards optimized triboelectric nanogenerators, *Nano Energy*, 2019, **62**, 530–549.
5 A. Kulandaivel, *et al.*, Advances in ferrofluid-based triboelectric nanogenerators: Design, performance, and prospects for energy harvesting applications, *Nano Energy*, 2024, **120**, 109110.

6 M. Yuan, *et al.*, Multifunctional subwavelength device for wide-band sound absorption and acoustic-electric conversion, *Sens. Actuators, A*, 2025, **389**, 116554.
7 C. Zhang, *et al.*, Wood-cellulose-fiber-based functional materials for triboelectric nanogenerators, *Nano Energy*, 2021, **81**, 105637.
8 T. Cheng, Q. Gao and Z. L. Wang, The current development and future outlook of triboelectric nanogenerators: a survey of literature, *Adv. Mater. Technol.*, 2019, **4**(3), 1800588.
9 Z. L. Wang, Triboelectric nanogenerators as new energy technology and self-powered sensors–Principles, problems and perspectives, *Faraday Discuss.*, 2014, **176**, 447–458.
10 Y. Song, *et al.*, Recent advances in cellulose-based piezoelectric and triboelectric nanogenerators for energy harvesting: a review, *J. Mater. Chem. A*, 2021, **9**(4), 1910–1937.
11 Y. Zhang, *et al.*, Multifunctional Sensitive Positive Friction Layer of TPU/MXene/STO Composited Film for Triboelectric Nanogenerator, *Nano Lett.*, 2025, **25**(14), 5713–5722.
12 Z. Li, *et al.*, Sustainable Biopolymers in Eco-Friendly Triboelectric Energy Harvesting, *Adv. Mater.*, 2025, **37**(22), 2412671.
13 Z. Liu, X. Chen and Z. L. Wang, Biopolymer and biomimetic techniques for triboelectric nanogenerators (TENGs), *Adv. Mater.*, 2025, **37**(22), 2409440.
14 R. Ankit and J. Kolte, Engineering of Chitosan/poly (vinyl alcohol) nanofibrous membrane as triboelectric nanogenerator for energy harvesting and self-powered speed sensor, *J. Mater. Sci.: Mater. Electron.*, 2025, **36**(22), 1366.
15 R. Ankit, T. Chakraborty and J. Kolte, Scalable Electrospun Chitosan/PVA Nanofibers: A Pathway for Triboelectric Nanogenerator-based Energy Harvesting, *Polymer*, 2025, 128848.
16 M. Shanbedi, H. Ardebili and A. Karim, Polymer-based triboelectric nanogenerators: Materials, characterization, and applications, *Prog. Polym. Sci.*, 2023, **144**, 101723.
17 S. Potu, *et al.*, Oxide based triboelectric nanogenerators: Recent advances and future prospects in energy harvesting, *Mater. Sci. Eng., R*, 2024, **161**, 100866.
18 C. Yao, *et al.*, Triboelectric nanogenerators and powerboards from cellulose nanofibrils and recycled materials, *Nano Energy*, 2016, **30**, 103–108.
19 Z. Niu, *et al.*, Recent advances in cellulose-based flexible triboelectric nanogenerators, *Nano Energy*, 2021, **87**, 106175.
20 D. Klemm, *et al.*, Cellulose: fascinating biopolymer and sustainable raw material, *Angew. Chem., Int. Ed.*, 2005, **44**(22), 3358–3393.
21 P. K. Annamalai, *et al.*, An overview of cellulose-based nanogenerators, *Adv. Mater. Technol.*, 2021, **6**(3), 2001164.
22 N. Wang, *et al.*, Dual-electric-polarity augmented cyanoethyl cellulose-based triboelectric nanogenerator with ultra-high triboelectric charge density and enhanced electrical output property at high humidity, *Nano Energy*, 2022, **103**, 107748.
23 T. Wang, *et al.*, Fully biodegradable water-soluble triboelectric nanogenerator for human physiological monitoring, *Nano Energy*, 2022, **93**, 106787.
24 J. Huang, *et al.*, Cellulose-Based Triboelectric Nanogenerator Prepared by Multi-Fluid Electrospinning for Respiratory Protection and Self-Powered Sensing, *Actuators*, 2024, **13**, 178.
25 Q. Zhu, *et al.*, Low-cost, environmentally friendly and high-performance cellulose-based triboelectric nanogenerator for self-powered human motion monitoring, *Cellulose*, 2022, **29**(16), 8733–8747.
26 C. Lin, *et al.*, An all paper based triboelectric nanogenerators with high output performance in extreme environment manufactured by multi-layer papers forming technology, *Chem. Eng. J.*, 2024, **488**, 151008.
27 S. Jakmuangpak, *et al.*, Engineering bacterial cellulose films by nanocomposite approach and surface modification for biocompatible triboelectric nanogenerator, *ACS Appl. Electron. Mater.*, 2020, **2**(8), 2498–2506.
28 S. U. Park, *et al.*, The possibility of microbial cellulose for dressing and scaffold materials, *Int. Wound J.*, 2014, **11**(1), 35–43.
29 L. Feng, *et al.*, A transparent and degradable bacterial cellulose-based film for triboelectric nanogenerator: Efficient biomechanical energy harvesting and human health monitoring, *Nano Energy*, 2024, **120**, 109068.
30 B. Rangaswamy, K. Vanitha and B. S. Hungund, Microbial cellulose production from bacteria isolated from rotten fruit, *Int. J. Polymer Sci.*, 2015, **2015**(1), 280784.
31 P. Bishop, *et al.*, Kombucha: Biochemical and microbiological impacts on the chemical and flavor profile, *Food Chem. Adv.*, 2022, **1**, 100025.
32 S. M. Choi, *et al.*, Bacterial cellulose and its applications, *Polymers*, 2022, **14**(6), 1080.
33 Z. Sun, *et al.*, Antibacterial films made of bacterial cellulose, *Polymers*, 2022, **14**(16), 3306.
34 B. Wei, G. Yang and F. Hong, Preparation and evaluation of a kind of bacterial cellulose dry films with antibacterial properties, *Carbohydr. Polym.*, 2011, **84**(1), 533–538.
35 F. Esa, S. M. Tasirin and N. Abd Rahman, Overview of bacterial cellulose production and application, *Agric. Sci. Proc.*, 2014, **2**, 113–119.
36 L. Segal, *et al.*, An empirical method for estimating the degree of crystallinity of native cellulose using the X-ray diffractometer, *Text. Res. J.*, 1959, **29**(10), 786–794.
37 S. Niu, *et al.*, Theoretical study of contact-mode triboelectric nanogenerators as an effective power source, *Energy Environ. Sci.*, 2013, **6**(12), 3576–3583.
38 S. K. Paswan, *et al.*, Electrical transport properties of nanocrystalline and bulk nickel ferrite using complex impedance spectroscopy: a comparative study, *Phys. Scr.*, 2022, **97**(9), 095812.
39 N. Atykyan, V. Revin and V. Shutova, Raman and FT-IR Spectroscopy investigation the cellulose structural differences from bacteria Gluconacetobacter sucrofermentans during the different regimes of cultivation on a molasses media, *AMB Express*, 2020, **10**(1), 84.
40 H. Suryanto, H. W. Wijaya and U. Yanuhar, FTIR analysis of alkali treatment on bacterial cellulose films obtained from pineapple peel juice, *IOP Conf. Ser.:Mater. Sci. Eng.*, 2021, **1034**(1), 012145.

41 R. Auta, *et al.*, Production and characterization of bacterial cellulose before and after enzymatic hydrolysis, *Afr. J. Biotechnol.*, 2017, **16**(10), 470–482.
42 M. Phisalaphong and N. Jatupaiboon, Biosynthesis and characterization of bacteria cellulose–chitosan film, *Carbohydr. Polym.*, 2008, **74**(3), 482–488.
43 Y. Qiu, *et al.*, Bacterial cellulose and bacterial cellulose-vaccarin membranes for wound healing, *Mater. Sci. Eng., C*, 2016, **59**, 303–309.
44 A. Vazquez, *et al.*, Bacterial cellulose from simple and low cost production media by Gluconacetobacter xylinus, *J. Polym. Environ.*, 2013, **21**, 545–554.
45 M. R. Levitt, *et al.*, Image-guided cerebrospinal fluid shunting in children: catheter accuracy and shunt survival, *J. Neurosurg. Pediatr.*, 2012, **10**(2), 112–117.
46 V. Zhong, *et al.*, Inhibition of diastatic yeasts by Saccharomyces killer toxins to prevent hyperattenuation during brewing, *Appl. Environ. Microbiol.*, 2024, **90**(10), e01072–24.
47 S. Lin, *et al.*, The overlapped electron-cloud model for electron transfer in contact electrification, *Adv. Funct. Mater.*, 2020, **30**(11), 1909724.
48 Y. Shao, *et al.*, Facile method to enhance output performance of bacterial cellulose nanofiber based triboelectric nanogenerator by controlling micro-nano structure and dielectric constant, *Nano Energy*, 2019, **62**, 620–627.
49 A. L. Freire, *et al.*, Metal-Free, Bio-Triboelectric Nanogenerator Based on a Single Electrode of Bacterial Cellulose Modified with Carbon Black, *Nanoenergy Adv.*, 2024, **4**(1), 110–121.